Geosci. Model Dev. Discuss., https://doi.org/10.5194/gmd-2019-1
Manuscript under review for journal Geosci. Model Dev.
Discussion started: 28 January 2019

Geoscientific Model Development Discussions

CAM6 simulation of mean and extreme precipitation over Asia: Sensitivity to upgraded physical parameterizations and higher horizontal resolution

Lei Lin[1], Andrew Gettelman[2], Yangyang Xu[3], Chenglai Wu[4], Zhili Wang[5], Wenjie Dong[1]

[1]School of Atmospheric Sciences and Guangdong Province Key Laboratory for Climate Change and Natural Disaster Studies, Sun Yat-sen University, Zhuhai, Guangdong, China
[2]National Center for Atmospheric Research, Boulder, Colorado, USA
[3]Department of Atmospheric Sciences, College of Geosciences, Texas A&M University, College Station, Texas, USA
[4]International Center for Climate and Environment Sciences, Institute of Atmospheric Physics, Chinese Academy of Sciences, Beijing, China
[5]State Key Laboratory of Severe Weather and Key Laboratory of Atmospheric Chemistry of CMA, Chinese Academy of Meteorological Sciences, Beijing, China

Correspondence to: Wenjie Dong (dongwj3@mail.sysu.edu.cn)

Abstract. The Community Atmosphere Model version 6 (CAM6) released in 2018, as part of the Community Earth System Model version 2 (CESM2) modeling framework, is a major upgrade over the previous CAM5 that has been used in numerous global and regional climate studies in the past six years. Since CESM2/CAM6 will participate in the upcoming Coupled Model Intercomparison Project phase 6 (CMIP6) and is likely to be adopted in many future studies, its simulation fidelity needs to be thoroughly examined. Here we evaluate the performance of a developmental version of the Community Atmosphere Model with parameterizations that will be used in CMIP6 (CAM6α) with the default 1° horizontal resolution (0.9° × 1.25°, CAM6α-1°) and a higher resolution simulation (approximately 0.25°, CAM6α-0.25°), against various precipitation observational datasets over Asia. The CAM6α performance is also compared with CAM5 with the default 1° horizontal resolution (CAM5-1°). With the prognostic treatment of precipitation processes (which is missing in CAM5) and the new microphysics module, CAM6 is able to better simulate climatological mean and extreme precipitation over Asia, to better capture the heaviest precipitation events, to reproduce the diurnal cycle of precipitation rates over most of Asia, and to better simulate the probability density distributions of daily precipitation over Tibet, Korea, Japan and Northern China. Higher horizontal resolution in CAM6α improves simulations of mean and extreme precipitation over mountainous Sichuan and Northern China, but the performance degrades over the Maritime continent. Further diagnosis on moisture budget suggests that the physical processes leading to model improvement are different over different regions. Both upgraded physical parameterizations and higher horizontal resolution affect the precipitation response to internal variability of ocean and atmosphere (e.g. Asian monsoon index, ENSO, PDO), but the effects vary across different regions. Higher horizontal resolution degrades the model performance in simulating precipitation variability associated with the East Asian summer monsoon in the middle and lower reaches of the Yangtze River in China. The precipitation variability associated with ENSO

Geosci. Model Dev. Discuss., https://doi.org/10.5194/gmd-2019-1
Manuscript under review for journal Geosci. Model Dev.
Discussion started: 28 January 2019

gets better with upgraded physical parameterizations and higher horizontal resolution. Higher horizontal resolution, however, induces an opposite response to PDO in CAM6 over Southern China.

1 Introduction

The Community Atmosphere Model (CAM) is an atmospheric general circulation model (AGCM) developed at the National Center for Atmospheric Research (NCAR) with extensive community support. The fifth version of CAM (CAM5) [*Neale et al*., 2010], as part of the Community Earth System Model version 1 (CESM1) [*Hurrell et al*., 2013], was widely used for climate studies over Asia. CAM5 included a two-moment cloud microphysics scheme that is missing in the previously CAM versions and improved the representation of low-level clouds [*Morrison and Gettelman*, 2008], net conversion rates from water vapor to cloud condensation [*Neale et al*., 2010; *Zhang et al*., 1995], and a three-mode aerosol module [*Liu et al*. 2012].

Among various applications, CESM1/CAM5 has been used in many studies regarding to clouds and precipitation over Asia. For example, *Zhang et al*. [2014] evaluated the sensitivity of simulated stratus clouds over eastern China to horizontal resolution in CAM5. *Zhang and Chen* [2016] investigated mean state and diurnal cycle of summer precipitation over continental East Asia in the CAM4 and CAM5 versions. *Li et al*. [2015] used CAM5 with different resolutions (2.8º, 1.0º and 0.45º, respectively) to study the impact of horizontal resolution on model performance in simulating precipitation over East Asia. *Wang et al*. [2018] investigated the sensitivity of Indian Summer Monsoon to different convective schemes in CAM5. *Jiang et al*. [2015] examined anthropogenic aerosol optical depths and their effects on clouds and precipitation in East Asia. *Vinoj et al*. [2014] found with CAM5 simulation that dust-induced atmospheric heating over North Africa and West Asia modulated monsoon rainfall over central India.

A pre-released version of CAM6 (denoted here as CAM6α, extensively tested in late 2017) shares the same basic physics as the released version of CAM6, except for slightly different tuning parameters and without the updated surface drag scheme. CAM6α was thoroughly evaluated over the continental United States [*Gettelman et al*., 2018], but its performance over predecessors remains unknown for Asia regions. Since CAM6 and other CMIP6 era models are likely to be used widely for hydroclimate studies over Asia in the next five to ten years, model fidelity needs to be carefully evaluated. For example, Global Atmosphere 6.0 (GA6), the latest atmosphere model from the UK Met Office, was used to study the interannual and intraseasonal precipitation variability over China [*Stephan et al*., 2018a and b]. GA6 includes a new dynamical core and updates various physical parameterizations [*Walters et al*., 2017]. Similarly, *Martin et al*. [2017] analyzed tropical precipitation in GA6 with a range of horizontal resolutions and found that the behaviour of the deep convection parameterization in GA6 is largely independent of the grid-box size and time step length over which it operates.

In addition to model physics upgrade, another area of growth in global climate model development is the enhancement of horizontal spatial resolution. The 0.25º (approximately 25 km) grid spacing is the targeted resolution for global atmosphere modeling in the near future [*Sharma et al*., 2016], while most of default CMIP6 runs at decadal to centennial

Geosci. Model Dev. Discuss., https://doi.org/10.5194/gmd-2019-1
Manuscript under review for journal Geosci. Model Dev.
Discussion started: 28 January 2019

scale are still set to 1º. Enhanced model resolution has been demonstrated as a means to reduce model biases *[Palmer*, 2014; *Yao et al*., 2017; *Chen et al*., 2018]. Several early studies have evaluated global model simulations at 0.23º (20km) resolution [*Oouchi et al*., 2006; *Kitoh and Kusunoki*, 2008]. Other CAM5 studies have also tested resolutions of 0.5º [*Bacmeister et al*., 2013; *Lau and Ploshay*, 2009] or 1º [*Zhang et al*., 2014; *Li et al*., 2015; *Lin et al., 2015*; *Lin et al*., 2016]. The performance of 0.25º CAM6 simulations over Asia has not been examined rigorously.

In order to provide insights on both physical schemes and horizontal resolution, here we analyze a three-model hierarchy. First, we explore the effects of new physical parameterizations by contrasting CAM6α-1º simulation with CAM5-1º. Second, we evaluate CAM6α with 1º and 0.25º resolution to quantify model sensitivity to horizontal resolution.

This technical model evaluation paper is divided into the following sections. After the introduction (Section 1), Section 2 provides detailed information on model configuration, model experiment set up, as well as observational datasets used as benchmarks. In Section 3, we compare climatological (multi-year) average of monthly mean and daily extreme precipitation simulated by three versions of CAM in the context of observational uncertainty. Section 4 is devoted to evaluation of precipitation variability at a wide range of time scales that is difficult to fine tune during model development process. Section 5 discusses in detail the improved climate simulation over two regions, attributed to new physical parameterizations and higher resolution, respectively. Finally, we present further discussion and summary in Section 6.

2 Methods

2.1 CAM simulation

The first set of simulation uses the publicly released version of CAM5.1 [*Neale et al*., 2010]. CAM5.1 treats stratus cloud microphysics with a double moment formulation of *Morrison and Gettelman* [2008] and *Gettelman et al*. [2008]. The spatial distribution of shallow convective activities is simulated with a set of realistic plume dilution equations [*Park and Bretherton*, 2009]. The ice cloud fraction scheme allows supersaturation via a modified relative humidity over ice and inclusion of ice condensation amount [*Gettelman et al*. 2010]. A three log-normal mode model was used to predict aerosol concentration, and the number concentration of aerosols are then connected to ice/warm cloud microphysics accounting for ice and liquid activation of cloud crystals and drops [*Liu et al*., 2012]. A Finite-Volume (FV) dynamical core (1º) is used.

The second and third sets of simulation considered in this study use a near-ready version of CAM6 (denoted as CAM6α) that has the same basic physics as the final version of CAM6 released in 2018 [*Bogenschutz et al*., 2013; *Gettelman et al*., 2018] but with slightly different tuning parameters. CAM6α used upgraded CLUBB [*Golaz et al*., 2002a and b], new ice nucleation parameterization [*Gettelman et al*., 2015; *Gettelman et al*., 2018], and modified aerosol modal model [*Liu et al*. 2016]. This model version, with the Spectral Element (SE) dynamical core [*Lauritzen et al*., 2018], was run twice with different horizontal resolutions (i.e., ~1º and ~0.25º). The same uniform resolution SE simulations with CAM6α forced by observed sea surface temperature data from 1980-2005 (saved output for monthly, daily and 3 hourly) are analyzed in *Gettelman et al*. [2018].

Geosci. Model Dev. Discuss., https://doi.org/10.5194/gmd-2019-1
Manuscript under review for journal Geosci. Model Dev.
Discussion started: 28 January 2019

All model simulations evaluated here (Table 1) followed the protocol of Atmospheric Model Intercomparison Project (AMIP). Simulations are forced by time-varying observed sea surface temperature and sea ice from 1979 to 2005, as well as evolution of aerosol emissions and trace gases concentration (including CO_2). The 25-year output during 1980-2004 are analyzed here to match with available observations. Monthly and daily frequency used.

2.2 Observational datasets

2.2.1 Asian Precipitation - Highly-Resolved Observational Data Integration Towards Evaluation (APHRODITE)

For the direct measurement of temperature and precipitation, APHRODITE data is used [*Yatagai et al.*, 2012]. APHRODITE is a gridded daily precipitation product covering monsoonal Asia, Middle East and Russia, and is available at 0.25º × 0.25º resolution during the period of 1951–2007. The dataset was created by collecting rain gauge measurements across Asia.

2.2.2 The Japanese 55-year reanalysis (JRA55)

The Japan Meteorological Agency (JMA) produced a reanlayais dataset (JRA55) using an operational data assimilation system with the 4D-Var scheme [*Kobayashi et al.*, 2015]. The dataset covers 55 years from 1958 (when regular radiosonde observation began on a global basis) to 2013. JRA55 has a horizontal resolution of 0.56°.

2.2.3 Modern-Era Retrospective analysis for Research and Applications version 2 (MERRA2)

MERRA2 is a NASA atmospheric reanalysis for the satellite era (from 1980 to present) using the Goddard Earth Observing System Model, Version 5 (GEOS-5) with its Atmospheric Data Assimilation System. MERRA2 has a spatial resolution 0.625º × 0.5º [*Gelaro et al.*, 2017]. We adopted MERRA2 as an additional benchmark specifically for daily precipitation evaluation, because of the well-known large uncertainty among various observational datasets [*Sheffield et al.*, 2012; *Trenberth et al.*, 2014].

2.2.4 Tropical Rainfall Measuring Mission (TRMM)

The latest TRMM 3B43 Version 7 data (0.25º) between 1998 and 2016, downloaded from NASA Goddard Space Flight Center, combines multiple independent precipitation estimates from TRMM Microwave Imager and Global Precipitation Climatology Centre rain gauge analysis. The 3-hourly record over Asia (unavailable in other three data sources) from 1999-2004 are used in our study to assess the diurnal cycle of precipitation [*Huffman*, 2013].

3 Climatological statistics of mean precipitation and daily extreme precipitation

Figure 1 shows the annual mean surface air temperature biases relative to APHRODITE. First note that although sharing some common surface measurements, the two observational datasets (JRA55 and APHRODITE) have major

differences over Tibet and southeast Asia regions (Figure 1a). We should not expect an atmospheric numerical model, which is only constrained at the surface by ocean temperature, to have a better performance in agreeing with the observational benchmark (APHRODITE here) than the reanalysis product (JRA55), which is fully constrained by both ground and atmospheric information. Thus, only areas over which the model-APHRODITE difference is larger than JRA55-APHRODITE difference are considered 'significant' and stippled in Figure 1b-d.

Similar to the difficulty in capturing the high-elevation temperature in JRA55, there is a warm bias over Eastern and Southern China and a cool bias over Tibet in the CAM5 simulations (Figure 1b). The cool bias over Tibet and warm bias over the foothill regions (both the Indian side and the northern edge of Tibet plateau) appear to be a long-standing issue for global and regional climate models. We note that the bias over Sichuan appears to be muted in the high-resolution version (Figure 1d), raising the promise of further enhancing the resolution.

Moreover, CAM6α reduces the temperature bias over southern China (Figure 1b-c). Over the entire domain considered in Figure 1, The RMSE relative to APHRODITE is 2.3℃ for CAM5-1˚, 2.4℃ for CAM6α-1˚ and 2.3℃ for CAM6α-0.25˚ (Note that RMSE for JRA55 is 1.5℃). The Root Mean Square Difference (RMSE) as a regional average quantity is not sufficient in characterizing the performance of model that varies at finer scale. Because of this limitation, in the following evaluation for precipitation, we divide the entire Asia into several regional boxes (Figure 2).

Figure 2 illustrates the climatological precipitation biases relative to APHRODITE. MERRA2 is considered here, as the third data source in addition to JRA55 and APHRODITE, to fully capture the larger uncertainty of observational datasets [*Herold et al*., 2015, 2016]. All three CAM simulations have a dry bias over the southern China and wet bias over the rest of China, especially Sichuan basin (near the eastern edge of Tibet Plateau) and also the Himalayan mountain range that defines the southern edge of Tibet Plateau. The precipitation bias in those regions are particularly concerning for two reasons: (a) many major rivers in East Asia, South Asia and Southeast Asia have their headwaters in those regions, (b) these regions are also prone to natural hazards such as landslides.

Overall, CAM6α-1º performance is slightly better than CAM5-1º, and CAM6α-0.25º falls in between the 1º resolution models (RMSE are 1.83 mm/day for CAM5-1º, 1.62 mm/day for CAM6α-1º and 1.71 mm/day for CAM6α-0.25º).

Because of the large spatial heterogeneity, eight regions are selected to evaluate precipitation. Five domains shown as the purple boxes of Figure 2c are Tibet, Sichuan, Korea, Japan and the Maritime Continent. The other three are India, Northern China and Southern China. Figure 3 shows RMSD and mean bias (the area average of model or dataset minus APHRODITE) of annual mean precipitation for eight selected regions. Note that over a few selected regions, the model performance is as good as reanalysis (such as over Japan, Korea and Southern China) and thus we will not further investigate the model improvement. Among regions where CAM models perform poorly compared with reanalysis (Sichuan, Tibet, India, Northern China and Maritime continent), CAM6α-1˚ performance (RMSD) is better (lower) than CAM5-1˚ for Tibet, Sichuan and Northern China, but gets worse for the Maritime continent. Notably, CAM6α-0.25˚ is closer to observations over Sichuan and Northern China, but also get considerably worse for the Maritime continent (with a large RMSE=7.2 mm/day and bias=4.0 mm/day).

Geosci. Model Dev. Discuss., https://doi.org/10.5194/gmd-2019-1
Manuscript under review for journal Geosci. Model Dev.
Discussion started: 28 January 2019

We will explore the details that might lead to the progressive improvement over Sichuan and Northern China in Section 5, while the poor performance of CAM6, especially over Maritime continent will be dealt with in a separate paper.

We next assess the model performance in simulating precipitation, separately, for convective and large-scale components. The ratio of convective and large-scale precipitation is a useful diagnostic, because both convective activity and large-scale instability can lead to precipitation in this model. Most atmospheric models use the convective parameterizations to balance large-scale thermal instabilities, and not to derive grid-scale microphysical and precipitation processes [*Zhang and McFarlane*, 1995; *Kooperman et al.* 2016]. The convective precipitation include the shallow and deep convective precipitation. In CAM6 shallow convective regime is handled by CLUBB coupled to stratiform microphysics and hence shallow convective precipitation is prognostic and part of the large scale precipitation.

The latent heating required by the atmosphere imposes an important constraint on the amount of mean rainfall, but model horizontal resolution and parameter settings decides the time scales [*Gustafson et al.* 2014]. CAM6 estimate the shallow convective precipitation from explicit prognostic calculation rather than diagnostically estimate from large-scale instabilities. One of the reason that the simulated rainfall intensity is expect to improve when the model run at higher resolution is small-scale processes actually simulated as opposed to to parameterizations would produce more rainfall [*Kopparla et al*., 2013].

The reanalysis product JRA55 also provides a decomposition of convective and large scale precipitation. (Figure 4a). Note that the convective and large-scale rainfall in JRA55 is not really observations and the partitioning is highly dependent on the JRA55 model assumptions. The ratio of convective (PRECC) to large-scale (PRECL) precipitation is greater over the ocean than over the land, as expected. CAM6α-1˚ has a larger ratio over the tropics, compared to CAM5-1º and JRA55 (Figure 4c). The CAM6α-0.25˚ simulated ratio is closer to JRA55, due to higher spatial resolution in both datasets (Figure 4d).

Higher horizontal resolution models tend to simulate higher vertical velocities [*Gettelman et al*., 2018] and a lower ratio of convective to total rainfall, because a larger fraction of precipitation can be resolved as the consequences of large-scale flow, limiting the need of invoking convective schemes. With a fixed amount of precipitable water, more condensation caused by the stratiform scheme means less is available for convective precipitation, so the ratio becomes lower.

In addition, the compensation above is a feature of the physical parameterization suite in CAM due to timescale. CLUBB and the prognostic cloud microphysics are run whenever large scale condensation that process removes all liquid supersaturation instantaneously. In contrast, the convective parameterization with a timescale produces mass flux and precipitation at a defined rate and consumes instability. The large scale condensation (including shallow convection and cloud microphysics) does more as the time step changes, while the deep convective parameterization does less. The high-resolution model has a shorter timestep (10 minutes vs. 30 minutes).

Figure 5 uses Taylor diagrams [*Taylor* 2001] to evaluate model performance of annual and seasonal surface air temperature, mean precipitation and two metrics of extreme precipitation. Red circles show the results from CAM5-1º, while blue for CAM6α-1º and green for CAM6α-0.25º. Movement closer to the point of (1.0, 1.0) in the Taylor diagrams indicates

Geosci. Model Dev. Discuss., https://doi.org/10.5194/gmd-2019-1
Manuscript under review for journal Geosci. Model Dev.
Discussion started: 28 January 2019

improvement of the simulation relative to APHRODITE. For example, the model circles are very close to the blue circles representing JRA55 for near-surface (2m) temperature (TREFHT) (Figure 5a), which indicates good performance for surface air temperature for all three models. The annual and seasonal precipitation (PRECT) correlations of the two CAM6α simulations are around 0.8, while the annual correlation of CAM5-1º is 0.7 (Figure 5b). CAM6α-0.25º RMS is bigger than that of CAM6α-1º (green circles relative to blue circles in Figure 5b). The maximum daily precipitation each month of a year (RX1day) of CAM6α-1º performance better than CAM5 (blue circles relative to red circles in Figure 5c). The number of heavy precipitation days (R10) shown large difference among three 'observation' data (black and gold circles in Figure 5d), but the two CAM6α has bigger correlation coefficients (~0.8) than CAM5 (~0.7).

Overall, CAM6α models have better performance than CAM5-1º for the mean precipitation (Figure 5b), maximum daily precipitation and number of heavy precipitation days values (Figure 5c and d). Although CAM6α-0.25º performance is worse than 1º for the mean precipitation and RX1day (green circles relative to blue circles in Figure 5b and c) mostly due to the bias over the Maritime Continent (not shown), CAM6α-0.25˚ performs better for R10 (Figure 5d). All three model versions show that precipitation bias in JJA is bigger than other seasons (Figure 5b and c).

4 Variability of simulated precipitation over Asian regions in various time scales

In this section, we evaluate simulated rainfall variability across a wide range of time scales. This serves as a useful test of model performance, because it is difficult to improve model performance in simulating temporal variability, as opposed to the climatological average, based on simple tuning of one or more parameters. Moreover, it is expected CAM6 will be widely used to study climate variability at various time scales.

4.1 Variability of precipitation due to PDO, ENSO and East Asia summer monsoon index

The Pacific Decadal Oscillation (PDO) represents variability in the tropical and extratropical North Pacific at interdecadal time scales that impact continental climate variables significantly [*Mantua et al*., 1997; *Meehl et al*., 2013]. Figure 6 shows a regression of annual precipitation in the observations and the models against the PDO index that derived as the leading principal component of monthly SST anomalies in the North Pacific Ocean [*Mantua et al*., 1997]. A common feature as revealed in the three observational records is the drying tendency over the Indochina Peninsula (e.g., Thailand) during positive PDO phases. This feature is well represented in all three CAM versions. Similarly, a wetting anomaly over most of India during positive PDO is also captured in CAM versions. In contrast, the wetting anomaly over Southern China is simulated well in the CAM6-0.25º version, while the opposite anomaly is seen in the CAM6α-1º.

El Niño / Southern Oscillation (ENSO) plays a central role in the ocean-atmosphere coupled interannual variability. CAM5 has been widely used to study ENSO impact over Asia [*Chen et al*., 2018; *Hoell et al*., 2016]. Figure 7 shows the regression coefficients between annual mean precipitation and ENSO (the cold tongue index used as the ENSO index in this study) [*Deser and Wallace*, 1987]. Both 1º CAM model (Figure 7d and e) capture the observed wetting anomaly over Pakistan and Afghanistan and drying anomaly over Indonesia. However, we find that the drying tendency over Southern

Geosci. Model Dev. Discuss., https://doi.org/10.5194/gmd-2019-1
Manuscript under review for journal Geosci. Model Dev.
Discussion started: 28 January 2019

China during El Nino years (the upper row of Figure 7) is completely missing in CAM5 but starts to emerge in CAM6α-1º version and gets better in CAM6α-0.25º version. Our results here thus call into questions of the fidelity of previous ENSO studies on hydroclimate over Southern China using CAM5.

Next, we examine precipitation variability associated with higher-frequency fluctuations due to East Asia Summer Monsoon (EASM). The EASM is an important climate system over East China. Climate models are used widely for EASM studies [*Zhou and Li*, 2002; *Chen et al*., 2010; *Zhou et al*., 2013], although model biases for the EASM are a long-lasting problem from CMIP3 (Coupled Model Intercomparison Project phase 3) to CMIP5 with limited improvement [*Song and Zhou*, 2014; *Kusunoki and Arakawa*, 2015]. The East Asia Summer Monsoon Index (EASMI) is a unified Dynamic Normalized Seasonality (DNS) monsoon index defined by *Li and Zeng* [2002, 2003]. This index is based on intensity of monthly wind field and can be used to depict both the seasonal cycle and inter-annual variability of monsoons. The EASMI for models are calculated from simulated wind field. Summer (June-July-August, JJA) mean is considered here.

Figure 8 shows regression coefficient between summer (June-July-August, JJA) precipitation in the East of China and EASMI. There is an apparent negative regression between EASMI and summer (JJA) rainfall in the middle and lower reaches of the Yangtze River in China for the observational and reanalysis data (Figure 8a-c). All three CAM models capture that positive correlation over Southern China (Figure 8d-f) found in the observations and reanalysis (Figure 8a-c), although two CAM6α shown the northern edge of the positive correlation is less more northward (about 2º latitude) than that of observational and reanalysis data (Figure 8e-f).

4.2 Seasonal cycle

Due to the monsoonal influence on both East Asia and South Asia, the summer precipitation dominates the annual total. Thus, the summer-winter contrast in precipitation serves as a useful quantity for model evaluation. JRA55 has less of a summer-winter contrast than APHRODITE (Figure 9a). Compared to APHRODITE, MERRA2 has almost the same annual cycle over China (Figure 9b). In CAM5, the JJA precipitation appears to be too large compared to the rest of the year. CAM6α-1º simulations reduce the bias in the annual cycle over Pakistan (Figure 9c and d), although models continue to overestimate seasonal variability over arid regions in western China. The seasonal variability is significantly improved in CAM6α-0.25º, especially along Himalaya mountain regions. Southern China, again, is a region where the CAM6-0.25º performance is improved substantially. This is further diagnosed in the next Figure.

In Figure 10, we show the time series of zonal mean precipitation between 100ºE and 125ºE to evaluate model performance in simulating the annual cycle of EASM related precipitation. Figure 10 shows that precipitation in a year mainly occurs from May to September, and rapidly shifts to Northern China around June and continue to September [*Su et al*., 2017].

It is clear that the APHRODITE, JRA55 and MERRA2 all depict such a northern shift (Figure 10a, b and c). Both versions of CAM6α capture this northern shift and the persistent from June to September, especially CAM6α-0.25º (Figure

10e and f), which is missing the persistent in CAM5-1º (the jumping cliff over July to August, Figure 10d). This explains the CAM5 deficiency as shown in Figure 9.

4.3 Day-to-day variability and diurnal cycle of precipitation

Figure 11 shows daily rainfall frequency distribution from renalaysis/observation and models. Despite large uncertainties among observational datasets, daily intensity for the CAM6-0.25˚ model (green line) is closer to observational values over Sichuan basin than other simulations (Figure 11b). CAM5-1˚ simulates a higher frequency of light precipitation (0.1-1.0 mm/day) over Korea, Japan, Northern China and Southern China (Figure 11a, c, d, g and h). New physical schemes in CAM6-1º capture the observational distribution over Korea and Japan (Figure 11c and d). Realistic rainfall intensity is not energetically necessary because more frequent weak events can produce the same latent heating as those less frequent but more intense rainfall events. The large-scale precipitation in CAM6 improves the light rainfall over Korea, Japan and Northern China (not shown).

To look into the heavy precipitation more carefully, Figure 12 shows the percentile precipitation from 90% to 99.99%, which captures the heaviest precipitation events [*Kooperman et al*., 2016]. CAM6 with new physics module (blue) lead to better performance over five of eight selected regions (Tibet, Sichuan, Japan, India, Northern and Southern China). Higher horizontal resolution (as in CAM6-0.25º, green) simulates better intensities over the Maritime Continent (Figure 12e), but the results degrade for the heaviest precipitation events over India, Northern and Southern China (Figure 12f-h).

Figure 13 shows the diurnal cycle of precipitation rates in June from TRMM satellite observations and model simulations. The satellite observations show that the diurnal peak in precipitation is around 20:00 (local time) over Tibet, India and the Maritime continent, while the peak over Southern China is in the afternoon (15:00 local time) (Figure 13a). CAM6α reproduces many features of the TRMM observations (Figure 13c and d), while CAM5-1º simulates an earlier-in-the-day peak precipitation over India, Southern China and Maritime continent (Figure 13b). CAM6α-0.25º simulates the diurnal cycle better than CAM6α-1º in the south of Tibet (Figure 13d) along the Himalayas. In general, CAM6 models have significant improvements over CAM5 in simulating diurnal cycle of precipitation in East Asia.

The CLUBB parameterization appears to be be the reason for this improvement. CLUBB has prognostic moments that provide memory that facilitate the initiation of shallow convection in the mid-morning and early afternoon. It is important to note that CLUBB improved simulation of the diurnal cycle is a robust feature in every development coupled and atmosphere-only simulation. The CLUBB unified parameterization is able to prevent the deep convective scheme from firing off too early and simulate a gradual transition of these regimes successfully [*Bogenschutz et al*., 2018].

5 Improvement due to physical parameterizations and high resolution: Northern China vs. Sichuan

We quantitatively contrast the climate variables over Sichuan and Northern China here, since the model with new physical module or high horizontal resolution both simulated precipitation climatology better over those two regions as seen in Figure 3.

Geosci. Model Dev. Discuss., https://doi.org/10.5194/gmd-2019-1
Manuscript under review for journal Geosci. Model Dev.
Discussion started: 28 January 2019

New physical modules and higher horizontal resolution perform better over Sichuan by decreasing the convective precipitation (-0.38 and -0.81 mm/day, respectively) but for different reasons. Less moisture available for precipitation induced by CLUBB might lead to the decrease in the convective precipitation over Sichuan. High-resolution simulations tend to decrease the energy used for the convective process (decreased latent heat flux and sensible heat flux), and thus decrease the convective precipitation.

New physics parameterizations in CAM6 simulate stronger solar flux reach the surface. This leads to more latent heat release, contributing to a decrease in the large scale precipitation by 0.25 mm/day. Better representation of topography at 0.23˚ resolution leads to increased downward shortwave flux at the surface in Northern China. Less convective precipitation associated with increased resolution is seen over Northern China by -0.31 mm/day. We also examine the moisture budget using diagnostics for precipitation changes [*Chou and Lan*, 2012]. The moisture budget analysis defines the mass conservation of water substance in an atmospheric column as:

$$\overline{P} + \overline{<\partial_x(uq)>} + \overline{<\partial_y(vq)>} + \mathrm{Re}\,s = \overline{E} \ , \qquad (1)$$

where P is precipitation, q is specific humidity, u (v) is zonal (meridional) wind and E is evaporation into atmosphere. <X> is a mass-weighted vertical integral and $\overline{X}$ demoted the temporal mean. The horizontal advection can be further decomposed into stationary and transient term based on:

$$X = \overline{X} + X' = [\overline{X}] + \overline{X}^* + X' \ , \qquad (2)$$

$[\overline{X}]$ ($\overline{X}^*$) are climatological zonal mean (stationary) eddy, X' is transient variation. See *Yao et al*. [*2017*] and *Chen et al*. [*2018*] for more details.

No significant difference on the evaporation is seen between the model and JRA55 data (Figure 14). The results indicate that CAM6 (both resolutions) simulates a moisture budget closer to JRA55 than CAM5-1º and the model precipitation bias appears mostly in the meridional moisture flux convergence term $(-\partial_y(\overline{vq}))$ over Sichuan (Figure 14a). Although a large residual over Northern China region (Figure 14b) may result from water vapor transport by the surface vertical movement induced by terrain slope [*Trenberth and Guillemot* 1995; *Seager et al*., 2010], all three version CAM and JRA55 shown the zonal mean of specific humidity eddy transport $[\overline{q}]$ dominates Northern China precipitation (Figure 14b).

6 Summary

Here we present a comprehensive evaluation of AMIP-style experiments from 1979 to 2004 using the Community Atmosphere Model version 5 and 6 prototype (CAM5 and CAM6α) at 0.25º and 1º spatial resolutions. CAM6 is very different from CAM5, because it has included a higher order closure scheme for the boundary layer, shallow convection and

cloud macrophysics. Other updates in CAM6 include prognostic precipitation in the microphysics, a four-mode aerosol model, and ice nucleation schemes. Shallow convection, cloud macrophysical parameterization schemes and planetary boundary layer in conventional physical packages may or may not be compatible with one another. The CLUBB parameterization in CAM6, instead, represents a "unified" parameterization that is responsible for boundary layer processes, warm cloud macrophysics and shallow convective processes. The explicit representation of shallow convection precipitation is interactively coupled to stratiform microphysics within CLUBB, which replaces the previous convective parameterizations that diagnose the large-scale instability and the convective response separately.

The major findings of this study are:

(1) For the climatology of mean precipitation over Asia, CAM6α-1º substantially reduces model biases. Using an observational dataset (APRHRODITE) as the baseline, the mean squared error is reduced by 11% in CAM6α-1º compared to CAM5-1º. In terms of spatial distribution, the most remarkable bias of CAM5 and CAM6 is excessive precipitation in the central China and rainfall deficit over South China.

(2) CAM6α better simulates the probability density distributions of daily precipitation over Tibet, Korea, Japan and Northern China. Specifically, CAM6α performs better for the frequency of daily light precipitation over Korea, Japan and Northern China and captures the heaviest precipitation events over most of Asia. Notably, CAM6α models capture the observed diurnal cycle of precipitation. With a prognostic treatment of large-scale instability and the convective response module, higher horizontal resolution leads to better performance over Sichuan basin (close to the edge of Tibet plateau) and Northern China for heavy precipitation.

(4) Upgraded physical modules decrease the simulated convective precipitation and reduces the total precipitation bias over Sichuan. More complex terrain leads to lower convective precipitation at higher resolution, which improves the model performance in the total precipitation over Sichuan and Northern China. Those improvements can be explained in terms of the meridional moisture convergence or zonal mean humidity eddy.

(5) Upgraded physical parameterizations and higher horizontal resolution substantially improves seasonal cycle of the precipitation. For temporal variability at different scales (decadal, interannual, seasonal, and diurnal), the model performance varies. Higher horizontal resolution degraded in simulate the negative correlation between Asian monsoon index and summer precipitation in the middle and lower reaches of the Yangtze River in China. CAM6α with 1º and 0.25º simulates the opposite anomaly during the positive PDO phases over Southern China. Upgraded physical parameterizations help with CAM to simulate the drying tendency over Southern China during El Nino years.

(6) CAM6 models generally have improvements over CAM5 in simulating diurnal cycle of precipitation in East Asia, due to the CLUBB parameterization. CLUBB has prognostic moments that provide memory that facilitate the initiation of shallow convection in the mid-morning and early afternoon.

Overall, CAM6 demonstrates a better performance over CAM5, but the model fidelity at regional scale still needs further improvement. Higher resolution improves CAM6 performance over Asia in many aspects, but some metrics are

degrading. Careful validation of its performance at regional scale is required before any quantitative statement about climate attribution and projection can be made.

Code availability

Model code released in CESM2 (http://www.cesm.ucar.edu/models/cesm2/). Download the current release code: git clone -b release-cesm2.1.0 https://github.com/ESCOMP/cesm.git.

Data availability

The model data for the results presented in this paper are archived at https://doi.org/10.5281/zenodo.2548255. Details about MERRA-2 can be found at http://gmao.gsf.nasa.gov/pubs/office_notes. http://www.chikyu.ac.jp/precip/ for APHRODITE. The observational EASMI is downloaded from: http://ljp.gcess.cn/dct/page/65577. ENSO index is from http://research.jisao.washington.edu/data/cti/. The PDO index is from: http://research.jisao.washington.edu/pdo/PDO.latest. TRMM is from https://pmm.nasa.gov/data-access/downloads/trmm.

Author contributions

WD and CW designed the study, LL led the analysis, AG performed CESM simulations, LL, YX and ZW prepared the manuscript with contributions from all co-authors.

Competing interests

The authors declare that they have no conflict of interest.

Acknowledgments

We thank Richard Neale in National Center for Atmospheric Research (NCAR) for the code for computing the diurnal cycle. We also thank Patrick Callaghan and Colin Zarzycki for assistance with the original CAM6 high resolution simulations. This study was supported by the National Key Research and Development Program of China (2016YFA0602701). The National Center for Atmospheric Research is supported by the U. S. National Science Foundation.

References

Bacmeister, J. T., Wehner, M. F., Neale, R. B., Gettelman, A., Hannay, C., Lauritzen, P. H., ... & Truesdale, J. E.: Exploratory high-resolution climate simulations using the Community Atmosphere Model (CAM), Journal of Climate, 27(9), 3073-3099, 2014.

Bogenschutz, P. A., Gettelman, A., Morrison, H., Larson, V. E., Craig, C., & Schanen, D. P.: Higher-order turbulence closure and its impact on climate simulations in the Community Atmosphere Model, Journal of Climate, 26(23), 9655-9676, 2013.

Bogenschutz, P. A., Gettelman, A., Hannay, C., Larson, V. E., Neale, R. B., Craig, C., & Chen, C. C.: The path to CAM6: coupled simulations with CAM5. 4 and CAM5. 5, Geoscientific Model Development, 11(1), 235, 2018.

Bretherton, C. S., & Park, S.: A new moist turbulence parameterization in the Community Atmosphere Model, Journal of Climate, 22(12), 3422-3448, 2009.

Chen, H., Zhou, T., Neale, R. B., Wu, X., & Zhang, G. J.: Performance of the new NCAR CAM3. 5 in East Asian summer monsoon simulations: Sensitivity to modifications of the convection scheme, Journal of Climate, 23(13), 3657-3675, 2010.

Chen, X., Wu, P., Roberts, M. J., & Zhou, T.: Potential Underestimation of Future Mei-Yu Rainfall with Coarse-Resolution Climate Models, Journal of Climate, 31(17), 6711-6727, 2018.

Chou, C., & Lan, C. W.: Changes in the annual range of precipitation under global warming, Journal of Climate, 25(1), 222-235, 2012.

Deser, C., & Wallace, J. M.: El Niño events and their relation to the Southern Oscillation: 1925–1986, Journal of Geophysical Research: Oceans, 92(C13), 14189-14196, 1987.

Gelaro, R., McCarty, W., Suárez, M. J., Todling, R., Molod, A., Takacs, L., ... & Wargan, K.: The modern-era retrospective analysis for research and applications, version 2 (MERRA-2), Journal of Climate, 30(14), 5419-5454, 2017.

Gettelman, A., Morrison, H., & Ghan, S. J.: A new two-moment bulk stratiform cloud microphysics scheme in the Community Atmosphere Model, version 3 (CAM3). Part II: Single-column and global results, Journal of Climate, 21(15), 3660-3679, 2008.

Gettelman, A., Liu, X., Ghan, S. J., Morrison, H., Park, S., Conley, A. J., ... & Li, J. L.: Global simulations of ice nucleation and ice supersaturation with an improved cloud scheme in the Community Atmosphere Model, Journal of Geophysical Research: Atmospheres, 115(D18), 2010.

Gettelman, A., & Morrison, H.: Advanced two-moment bulk microphysics for global models. Part I: Off-line tests and comparison with other schemes, Journal of Climate, 28(3), 1268-1287, 2015.

Gettelman, A., Bresch, D. N., Chen, C. C., Truesdale, J. E., & Bacmeister, J. T.: Projections of future tropical cyclone damage with a high-resolution global climate model, Climatic Change, 146(3-4), 575-585, 2018.

Ghan, S. J., Liu, X., Easter, R. C., Zaveri, R., Rasch, P. J., Yoon, J. H., & Eaton, B.: Toward a minimal representation of aerosols in climate models: Comparative decomposition of aerosol direct, semidirect, and indirect radiative forcing, Journal of Climate, 25(19), 6461-6476, 2012.

Golaz, J. C., Larson, V. E., & Cotton, W. R.: A PDF-based model for boundary layer clouds. Part I: Method and model description, Journal of the atmospheric sciences, 59(24), 3540-3551, 2002a.

Golaz, J. C., Larson, V. E., & Cotton, W. R.: A PDF-based model for boundary layer clouds. Part II: Model results, Journal of the atmospheric sciences, 59(24), 3552-3571, 2002b.

Guo, H., Golaz, J. C., Donner, L. J., Wyman, B., Zhao, M., & Ginoux, P.: CLUBB as a unified cloud parameterization: Opportunities and challenges, Geophysical Research Letters, 42(11), 4540-4547, 2015.

Gustafson Jr, W. I., Ma, P. L., & Singh, B.: Precipitation characteristics of CAM5 physics at mesoscale resolution during MC3E and the impact of convective timescale choice, Journal of Advances in Modeling Earth Systems, 6(4), 1271-1287, 2014.

Hoell, A., Hoerling, M., Eischeid, J., Wolter, K., Dole, R., Perlwitz, J., ... & Cheng, L.: Does El Niño intensity matter for California precipitation?, Geophysical Research Letters, 43(2), 819-825, 2016.

Huffman, G. J., & Bolvin, D. T.: TRMM and other data precipitation data set documentation, NASA, Greenbelt, USA, 28, 2013.

Hurrell, J. W., Holland, M. M., Gent, P. R., Ghan, S., Kay, J. E., Kushner, P. J., ... & Lipscomb, W. H.: The community earth system model: a framework for collaborative research, Bulletin of the American Meteorological Society, 94(9), 1339-1360, 2013.

Jiang, Y., Yang, X. Q., & Liu, X.: Seasonality in anthropogenic aerosol effects on East Asian climate simulated with CAM5, Journal of Geophysical Research: Atmospheres, 120(20), 10-837, 2015.

Kitoh, A., & Kusunoki, S.: East Asian summer monsoon simulation by a 20-km mesh AGCM, Climate Dynamics, 31(4), 389-401, 2008.

Kobayashi, S., Ota, Y., Harada, Y., Ebita, A., Moriya, M., Onoda, H., ... & Miyaoka, K.: The JRA-55 reanalysis: General specifications and basic characteristics, Journal of the Meteorological Society of Japan. Ser. II, 93(1), 5-48, 2015.

Kooperman, G. J., Pritchard, M. S., Burt, M. A., Branson, M. D., & Randall, D. A.: Robust effects of cloud superparameterization on simulated daily rainfall intensity statistics across multiple versions of the Community Earth System Model, Journal of Advances in Modeling Earth Systems, 8(1), 140-165, 2016.

Kopparla, P., Fischer, E. M., Hannay, C., & Knutti, R.: Improved simulation of extreme precipitation in a high-resolution atmosphere model, Geophysical Research Letters, 40(21), 5803-5808, 2013.

Kusunoki, S., & Arakawa, O.: Are CMIP5 models better than CMIP3 models in simulating precipitation over East Asia?, Journal of Climate, 28(14), 5601-5621, 2015.

Lau, N. C., & Ploshay, J. J.: Simulation of synoptic-and subsynoptic-scale phenomena associated with the East Asian summer monsoon using a high-resolution GCM, Monthly Weather Review, 137(1), 137-160, 2009.

Lauritzen, P. H., Nair, R. D., Herrington, A. R., Callaghan, P., Goldhaber, S., Dennis, J. M., ... & Ullrich, P. A.: NCAR Release of CAM-SE in CESM2. 0: A Reformulation of the Spectral Element Dynamical Core in Dry-Mass Vertical Coordinates With Comprehensive Treatment of Condensates and Energy, Journal of Advances in Modeling Earth Systems, 10(7), 1537-1570, 2018.

Li, J., & Zeng, Q.: A unified monsoon index, Geophysical Research Letters, 29(8), 115-1, 2002.

Jianping, L., & Qingcun, Z.: A new monsoon index and the geographical distribution of the global monsoons, Advances in Atmospheric Sciences, 20(2), 299-302, 2003.

Li, J., Yu, R., Yuan, W., Chen, H., Sun, W., & Zhang, Y.: Precipitation over East Asia simulated by NCAR CAM5 at different horizontal resolutions, Journal of Advances in Modeling Earth Systems, 7(2), 774-790, 2015.

Lin, L., Gettelman, A., Feng, S., & Fu, Q.: Simulated climatology and evolution of aridity in the 21st century, Journal of Geophysical Research: Atmospheres, 120(12), 5795-5815, 2015.

Lin, L., Gettelman, A., Fu, Q., & Xu, Y.: Simulated differences in 21st century aridity due to different scenarios of greenhouse gases and aerosols, Climatic Change, 146(3-4), 407-422, 2016.

Liu, X., Easter, R. C., Ghan, S. J., Zaveri, R., Rasch, P., Shi, X., ... & Conley, A.: Toward a minimal representation of aerosols in climate models: Description and evaluation in the Community Atmosphere Model CAM5, Geoscientific Model Development, 5(3), 709, 2012.

Liu, X., Ma, P. L., Wang, H., Tilmes, S., Singh, B., Easter, R. C., ... & Rasch, P. J.: Description and evaluation of a new four-mode version of the Modal Aerosol Module (MAM4) within version 5.3 of the Community Atmosphere Model, Geoscientific Model Development (Online), 9(PNNL-SA-110649), 2016.

Mantua, N. J., Hare, S. R., Zhang, Y., Wallace, J. M., & Francis, R. C.: A Pacific interdecadal climate oscillation with impacts on salmon production, Bulletin of the american Meteorological Society, 78(6), 1069-1080, 1997.

Martin, G. M., Klingaman, N. P., & Moise, A. F.: Connecting spatial and temporal scales of tropical precipitation in observations and the MetUM-GA6, Geoscientific Model Development, 10(1), 105-126, 2017.

Meehl, G. A., Hu, A., Arblaster, J. M., Fasullo, J., & Trenberth, K. E.: Externally forced and internally generated decadal climate variability associated with the Interdecadal Pacific Oscillation, Journal of Climate, 26(18), 7298-7310, 2013.

Morrison, H., & Gettelman, A.: A new two-moment bulk stratiform cloud microphysics scheme in the Community Atmosphere Model, version 3 (CAM3), Part I: Description and numerical tests, Journal of Climate, 21(15), 3642-3659, 2008.

Neale, R. B., Chen, C. C., Gettelman, A., Lauritzen, P. H., Park, S., Williamson, D. L., ... & Marsh, D.: Description of the NCAR community atmosphere model (CAM 5.0), NCAR Tech. Note NCAR/TN-486+ STR, 1(1), 1-12, 2010.

Oouchi, K., Yoshimura, J., Yoshimura, H., Mizuta, R., Kusunoki, S., & Noda, A.: Tropical cyclone climatology in a global-warming climate as simulated in a 20 km-mesh global atmospheric model: Frequency and wind intensity analyses, Journal of the Meteorological Society of Japan. Ser. II, 84(2), 259-276, 2006.

Palmer, T.: Climate forecasting: Build high-resolution global climate models, Nature News, 515(7527), 338, 2014.

Park, S., & Bretherton, C. S.: The University of Washington shallow convection and moist turbulence schemes and their impact on climate simulations with the Community Atmosphere Model, Journal of Climate, 22(12), 3449-3469, 2009.

Park, S., Bretherton, C. S., & Rasch, P. J.: Integrating cloud processes in the Community Atmosphere Model, version 5, Journal of Climate, 27(18), 6821-6856, 2014.

Seager, R., Naik, N., & Vecchi, G. A.: Thermodynamic and dynamic mechanisms for large-scale changes in the hydrological cycle in response to global warming, Journal of Climate, 23(17), 4651-4668, 2010.

Sharma, V., Kilic, A., & Irmak, S.: Impact of scale/resolution on evapotranspiration from Landsat and MODIS images, Water Resources Research, 52(3), 1800-1819, 2016.

Sheffield, J., Wood, E. F., & Roderick, M. L.: Little change in global drought over the past 60 years, Nature, 491(7424), 435, 2012.

Shi, Y., Zhang, J., Reid, J. S., Liu, B., & Hyer, E. J.: Critical evaluation of cloud contamination in the MISR aerosol products using MODIS cloud mask products, Atmospheric Measurement Techniques, 7(6), 1791-1801, 2014.

Song, F., & Zhou, T.: The crucial role of internal variability in modulating the decadal variation of the East Asian summer monsoon–ENSO relationship during the twentieth century, Journal of Climate, 28(18), 7093-7107, 2015.

Su Tonghua, Xue Feng, Chen Minyan, et al.: A mechanism study for the intraseasonal oscillation impact on the two northward jumps of the western Pacific subtropical high, Chinese Journal of Atmospheric Sciences (in Chinese), 41 (3): 437–460, doi:10.3878/j.issn.1006-9895.1609.16125, 2017.

Stephan, C. C., Klingaman, N. P., Vidale, P. L., Turner, A. G., Demory, M. E., & Guo, L.: Interannual rainfall variability over China in the MetUM GA6 and GC2 configurations, Geoscientific Model Development, 11(5), 1823, 2018a.

Stephan, C. C., Ng, Y. H., & Klingaman, N. P.: On Northern HemisphereWave Patterns Associated with Winter Rainfall Events in China, Advances in Atmospheric Sciences, 35(8), 1021-1034, 2018b.

Taylor, K. E.: Summarizing multiple aspects of model performance in a single diagram, Journal of Geophysical Research: Atmospheres, 106(D7), 7183-7192, 2001.

Trenberth, K. E., & Guillemot, C. J.: Evaluation of the global atmospheric moisture budget as seen from analyses, Journal of Climate, 8(9), 2255-2272, 1995.

Trenberth, K. E., Dai, A., Van Der Schrier, G., Jones, P. D., Barichivich, J., Briffa, K. R., & Sheffield, J.: Global warming and changes in drought, Nature Climate Change, 4(1), 17, 2014.

Vinoj, V., Rasch, P. J., Wang, H., Yoon, J. H., Ma, P. L., Landu, K., & Singh, B.: Short-term modulation of Indian summer monsoon rainfall by West Asian dust, Nature Geoscience, 7(4), 308-313, 2014.

Walters, D., Brooks, M., Boutle, I., Melvin, T., Stratton, R., Vosper, S., ... & Bushell, A.: The Met Office unified model global atmosphere 6.0/6.1 and JULES global land 6.0/6.1 configurations, Geoscientific Model Development, 10(4), 1487-1520, 2017.

Wang, Y., Zhang, G. J., & Jiang, Y.: Linking stochasticity of convection to large-scale vertical velocity to improve Indian summer monsoon simulation in the NCAR CAM5, Journal of Climate, 31(17), 6985-7002, 2018.

Yao, J., Zhou, T., Guo, Z., Chen, X., Zou, L., & Sun, Y.: Improved performance of high-resolution atmospheric models in simulating the East Asian summer monsoon rain belt, Journal of Climate, 30(21), 8825-8840, 2017.

Yatagai, A., Kamiguchi, K., Arakawa, O., Hamada, A., Yasutomi, N., & Kitoh, A.: APHRODITE: Constructing a long-term daily gridded precipitation dataset for Asia based on a dense network of rain gauges, Bulletin of the American Meteorological Society, 93(9), 1401-1415, 2012.

Zhang, G. J., & McFarlane, N. A.: Sensitivity of climate simulations to the parameterization of cumulus convection in the Canadian Climate Centre general circulation model, Atmosphere-ocean, 33(3), 407-446, 1995.

Zhang, C., Wang, M., Morrison, H., Somerville, R. C., Zhang, K., Liu, X., & Li, J. L. F.: Investigating ice nucleation in cirrus clouds with an aerosol-enabled Multiscale Modeling Framework, Journal of Advances in Modeling Earth Systems, 6(4), 998-1015, 2014.

Zhang, X., Alexander, L., Hegerl, G. C., Jones, P., Tank, A. K., Peterson, T. C., ... & Zwiers, F. W.: Indices for monitoring changes in extremes based on daily temperature and precipitation data, Wiley Interdisciplinary Reviews: Climate Change, 2(6), 851-870, 2011.

Zhang, Y., Chen, H., & Yu, R.: Simulations of stratus clouds over eastern China in CAM5: Sensitivity to horizontal resolution, Journal of Climate, 27(18), 7033-7052, 2014.

Zhang, Y., & Chen, H.: Comparing CAM5 and superparameterized CAM5 simulations of summer precipitation characteristics over continental East Asia: Mean state, frequency–intensity relationship, diurnal cycle, and influencing factors, Journal of Climate, 29(3), 1067-1089, 2016.

Zhou, T. J., & Li, Z.: Simulation of the East Asian summer monsoon using a variable resolution atmospheric GCM, Climate Dynamics, 19(2), 167-180, 2002.

Zhou, T., Song, F., Lin, R., Chen, X., & Chen, X.: The 2012 North China floods: Explaining an extreme rainfall event in the context of a longer-term drying tendency, Bulletin of the American Meteorological Society, 94(9), S49, 2013.

Geosci. Model Dev. Discuss., https://doi.org/10.5194/gmd-2019-1
Manuscript under review for journal Geosci. Model Dev.
Discussion started: 28 January 2019

	CAM5-1º	CAM6α-1º	CAM6α-0.25º
Deep convection	ZM1995	ZM1995	ZM1995
Shallow convection	PB2009	CLUBB	CLUBB
Planetary boundary layer	BP2009	CLUBB	CLUBB
Warm cloud macrophysics	P2014	CLUBB	CLUBB
Ice cloud macrophysics	G2010	G2010	G2010
Cloud Microphysics	MG1	MG2	MG2
Aerosols	MAM3	MAM4	MAM4
Horizontal resolution (latitude * longitude)	0.9º × 1.25º	0.9º × 1.25º	0.23º × 0.31º

Table 1. Three CAM versions with major physical schemes listed in abbreviations. ZM1995 is *Zhang and McFarlane* [1995]. PB2009 is *Park and Bretherton* [2009]. BP2009 is *Bretherton and Park* [2009]. P2014 is *Park et al.* [2014]. MG1 is *Morrison and Gettelman* [2008]. MG2 is *Gettelman and Morrison* [2015]. G2010 is *Gettelman et al.* [2010]. CLUBB is *Golaz et al.* [2002a]. MAM3 is *Liu et al.* [2012]. MAM4 is *Liu et al.* [2016].

Geosci. Model Dev. Discuss., https://doi.org/10.5194/gmd-2019-1
Manuscript under review for journal Geosci. Model Dev.
Discussion started: 28 January 2019

Geoscientific Model Development Discussions

Differences due to physical parameterizations and high resolution	Sichuan		Northern China	
	Physic P.	High Res.	Physic P.	High Res.
TREFHT (℃)	-0.21	**-0.42**[a]	-0.01	**0.48**
LHFLX (W/m^2)	**2.28**	**-4.03**	**2.24**	**-1.86**
SHFLX (W/m^2)	**-3.73**	**-7.37**	0.10	**1.73**
FSDSC (W/m^2)	-0.48	**-3.03**	**-1.23**	**-3.46**
FSDS (W/m^2)	**7.08**	**5.32**	**3.38**	**2.87**
FLDS (W/m^2)	**-5.75**	**-4.00**	0.08	-0.12
CLDTOT (%)	**-1.46**	0.51	0.56	-0.68
INT_Q (kg/kg)	**-0.12**	-0.01	-0.13	0.04
PRECT (mm/day)	**-0.44**	**-1.06**	-0.24	-0.12
PRECC (mm/day)	**-0.38**	**-0.81**	0.01	**-0.31**
PRECL (mm/day)	-0.06	-0.25	**-0.25**	0.19

Table 2. Simulation differences due to physical parameterizations (CAM6α-1° minus CAM5-1°) and high horizontal resolution (CAM6α-0.25° minus CAM6α-1°), respectively. The values are averages over Sichuan and Northern China during 1980-2004. TREFHT: Surface air temperature; LHFLX: Surface latent heat flux; SHFLX: Surface sensible heat flux; FSDSC: Clearsky downwelling solar flux at surface; FSDS: Downwelling solar flux at surface; FLDS:

Geosci. Model Dev. Discuss., https://doi.org/10.5194/gmd-2019-1
Manuscript under review for journal Geosci. Model Dev.
Discussion started: 28 January 2019

Geoscientific Model Development Discussions

Downwelling longwave flux at surface; CLDTOT: Vertically-integrated total cloud; INT_Q: Vertically-integrated humidity; PRECT: Total precipitation rate; PRECC: Convective precipitation rate; PRECL: Large-scale precipitation rate.

[a] Statistically significant differences are emphasized in bold (95% confidence level from a two-sided t test).

5

Geosci. Model Dev. Discuss., https://doi.org/10.5194/gmd-2019-1
Manuscript under review for journal Geosci. Model Dev.
Discussion started: 28 January 2019

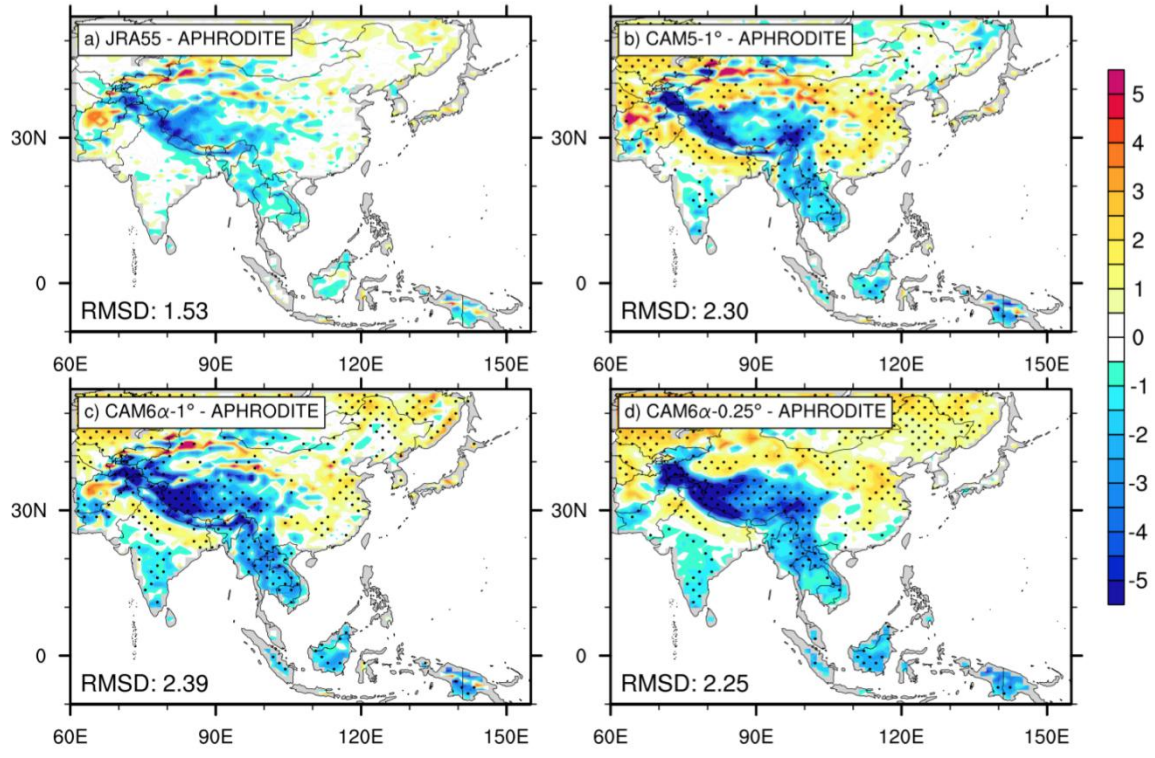

Figure 1. The difference of 1980-2004 annual mean surface air temperature (°C) between observation (APHRODITE) and (a) JRA55, (b) CAM5-1°, (c) CAM6α-1° and (d) CAM6α-0.25°, respectively. The values at the lower left of each panel indicate the root mean squared difference (RMSD) relative to APHRODITE. Grid points in panel (b)-(d) are stippled if the absolute difference between the respective model and APHRODITE is larger than that between JRA55 and APHRODITE.

Geosci. Model Dev. Discuss., https://doi.org/10.5194/gmd-2019-1
Manuscript under review for journal Geosci. Model Dev.
Discussion started: 28 January 2019

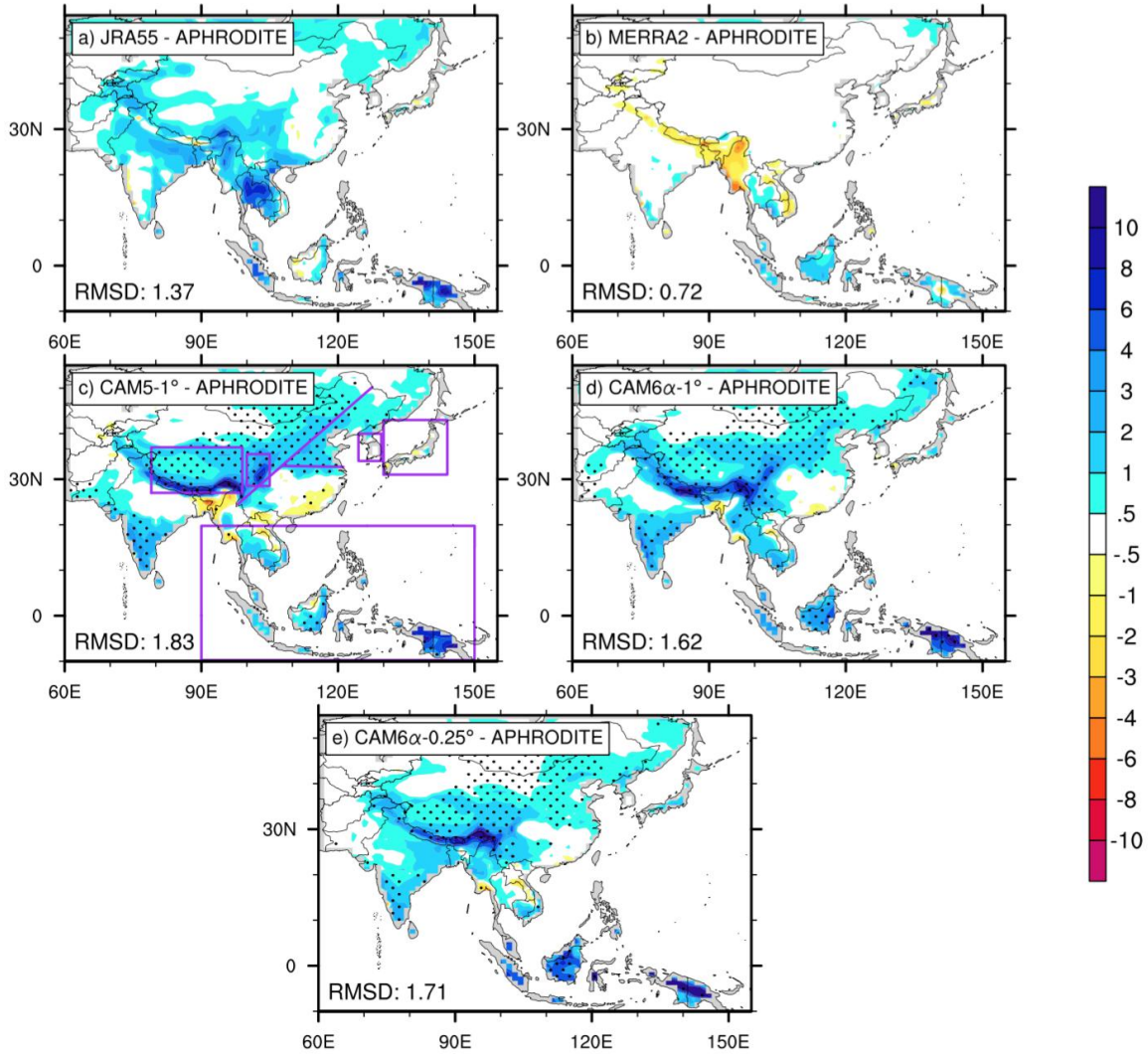

Figure 2. The difference of 1980-2004 annual mean precipitation (mm/day) between APHRODITE and (a) JRA55, (b) MERRA2, (c) CAM5-1º, (d) CAM6α-1º and (e) CAM6α-0.25º, respectively. The values at the lower left of each panel indicate the root mean squared difference (RMSD) relative to APHRODITE. Grid points in panel (c)-(e) are stippled when the absolute difference between model and APHRODITE is larger than that of between JRA55 and APHRODITE.

Geosci. Model Dev. Discuss., https://doi.org/10.5194/gmd-2019-1
Manuscript under review for journal Geosci. Model Dev.
Discussion started: 28 January 2019

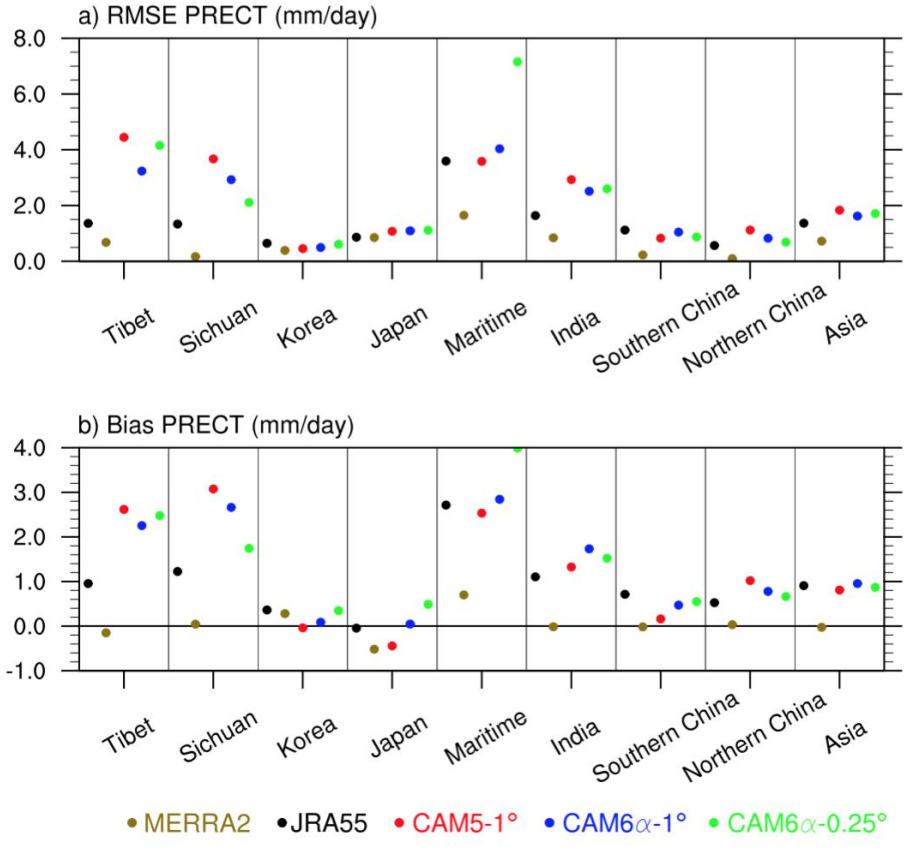

Figure 3. The root mean squared difference (RMSD) and bias of annual mean precipitation (PRECT, mm/day) relative to APHRODITE for JRA55, MERRA2, CAM5-1º, CAM6α-1º and CAM6α-0.25º over 8 regions: Tibet: 27°N–37°N, 79°E–99°E; Sichuan: 28.5°N–35.5°N, 100°E–105°E; Korea: 34°N–40°N, 124.5°E–129.5°E; Japan: 31°N–43°N, 130°E–144°E; Maritime: 9.75°S–19.75°N, 90°E–150°E; Asia: 5°N–55°N, 60°E–140°E. Three other domains are following geographical boundary and climatic zones for India, Northern China and Southern China as in Lin et al. [2018]. The "India" average is the entirely within mainland India. The western boundary of "Northern China" and "Southern China" is a straight line (shown in Figure 2c) named "Hu-Huanyong Line" between Heihe (50.2°N, 127.5°E) and Tengchong (24.5°N, 98.0°E). The separation of "Northern China" and "Southern China" (shown as the straight line in Figure 2c) is along the latitude of "Qin-Mountain and Huai-River" (32.8°N), with the northern part traditionally considered as semi-arid regions receiving less than 800 mm/year of precipitation.

Geosci. Model Dev. Discuss., https://doi.org/10.5194/gmd-2019-1
Manuscript under review for journal Geosci. Model Dev.
Discussion started: 28 January 2019

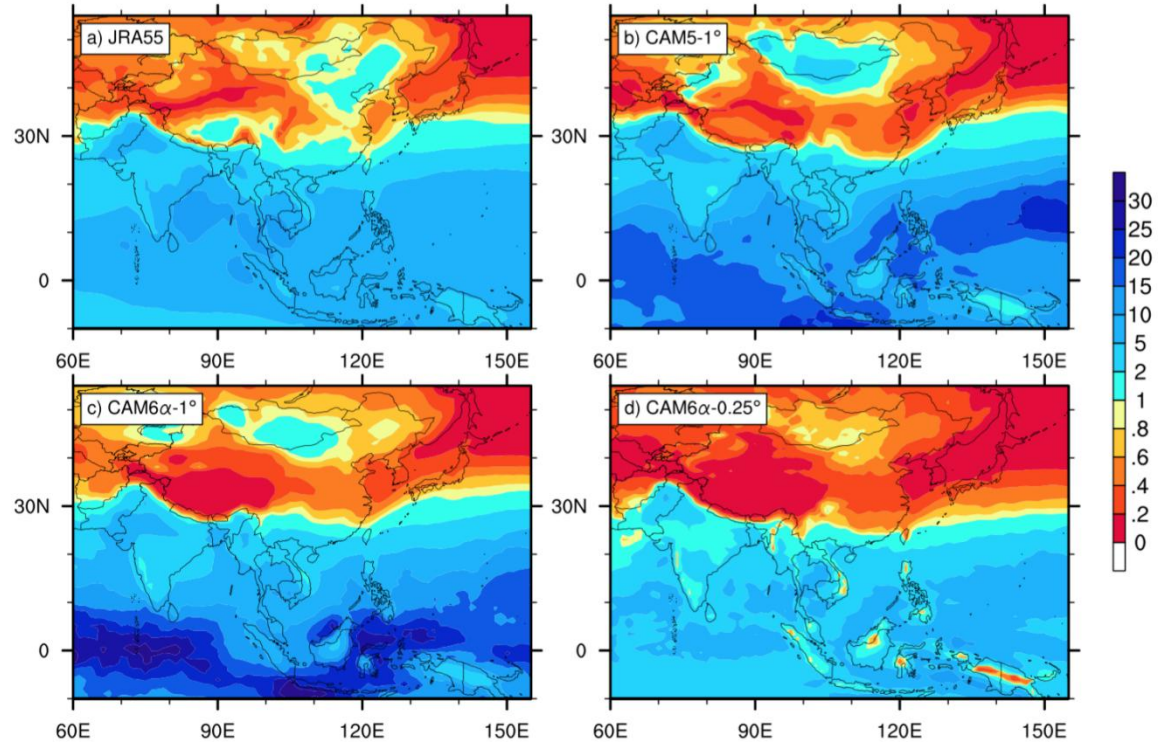

Figure 4. The 1980-2004 convective / large-scale precipitation ratio (unitless) for the a) JRA55, b) CAM5-1°, c) CAM6α-1° and d) CAM6α-0.25°, respectively.

Geosci. Model Dev. Discuss., https://doi.org/10.5194/gmd-2019-1
Manuscript under review for journal Geosci. Model Dev.
Discussion started: 28 January 2019

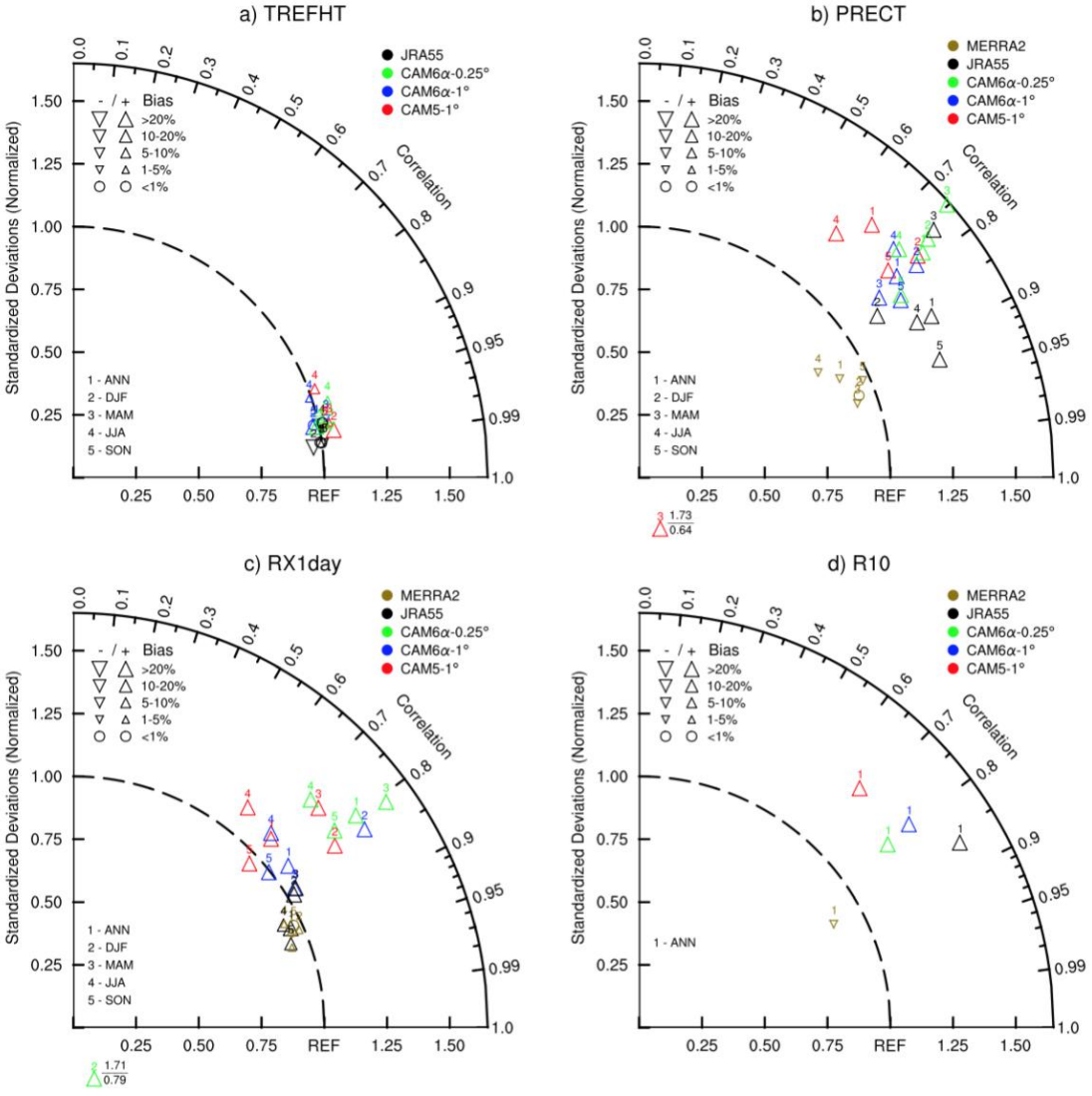

Figure 5. Taylor diagrams for (a) surface air temperature, (b) precipitation, (c) RX1day (the maximum daily precipitation during each month of a year, units: mm/day), (d) R10 (number of days with precipitation more than 10 mm, units: days). These two extreme indices are suggested by the Expert Team for Climate Change Detection and Indices [Zhang et al., 2011]. Note that R10, by design, only has annual mean, but not seasonal mean. Spatial correlations and normalized RMS (root mean square) are calculated for ANN (with 1 on the top), DJF (2, winter), MAM (3, spring), JJA (4, summer), SON (5, fall). APHRODITE is used as the benchmark over Asia for 1980-2004.

Geosci. Model Dev. Discuss., https://doi.org/10.5194/gmd-2019-1
Manuscript under review for journal Geosci. Model Dev.
Discussion started: 28 January 2019

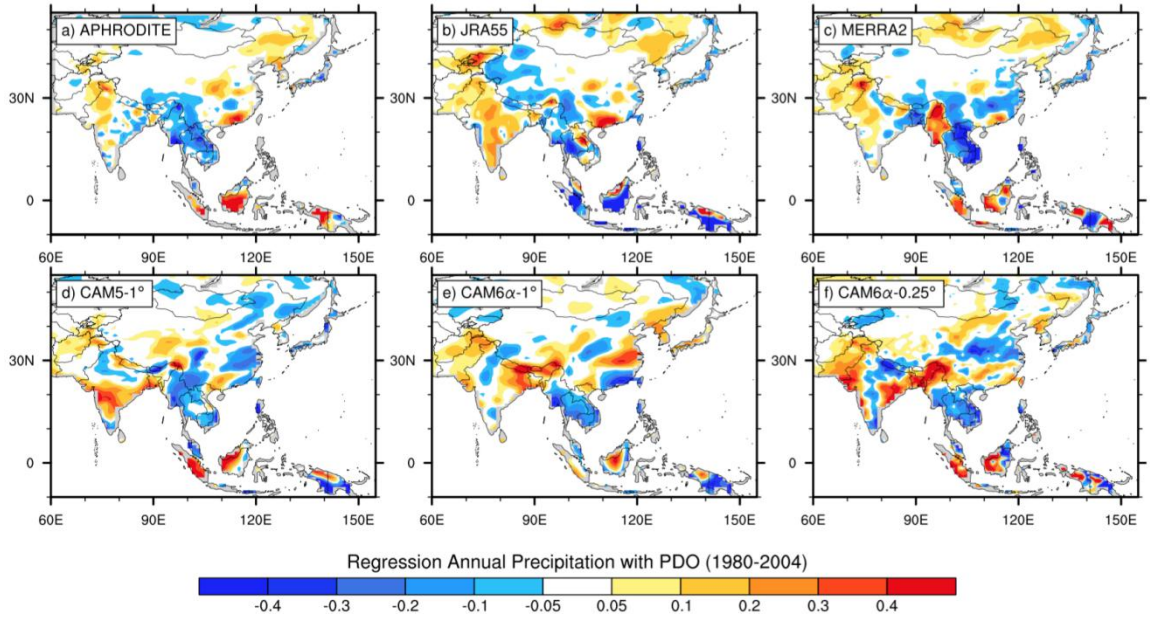

Figure 6. Annual mean precipitation (mm/day) regressed onto observed PDO indices for 1980-2004.

Geosci. Model Dev. Discuss., https://doi.org/10.5194/gmd-2019-1
Manuscript under review for journal Geosci. Model Dev.
Discussion started: 28 January 2019

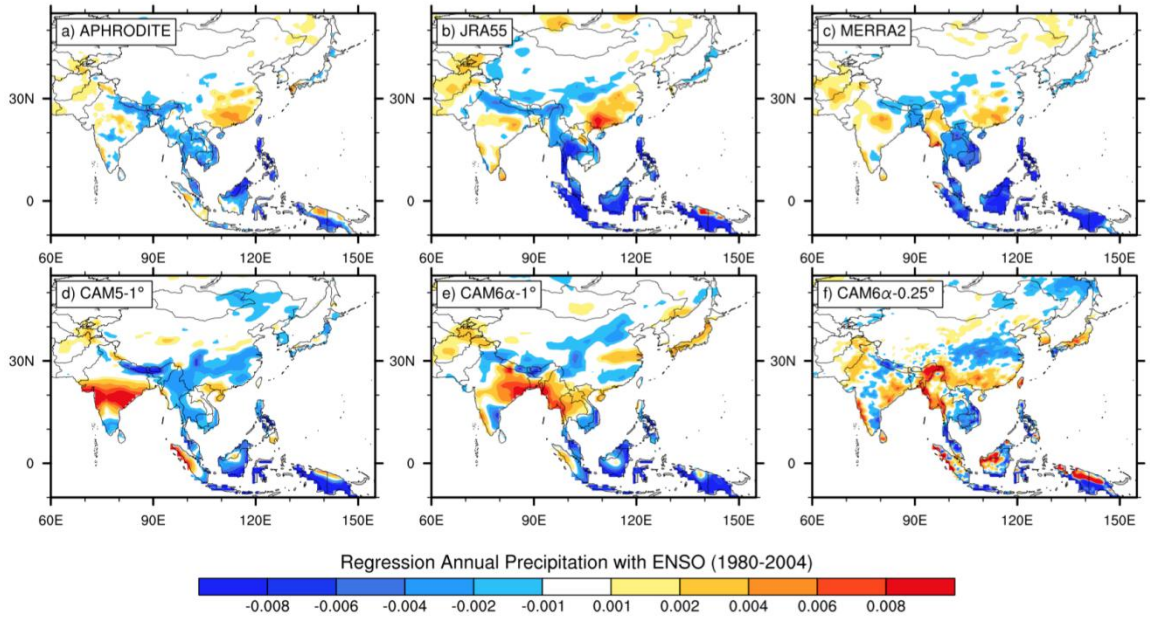

Figure 7. Annual mean precipitation regressed onto the observed ENSO index (mm/day) for 1980-2004.

Geosci. Model Dev. Discuss., https://doi.org/10.5194/gmd-2019-1
Manuscript under review for journal Geosci. Model Dev.
Discussion started: 28 January 2019

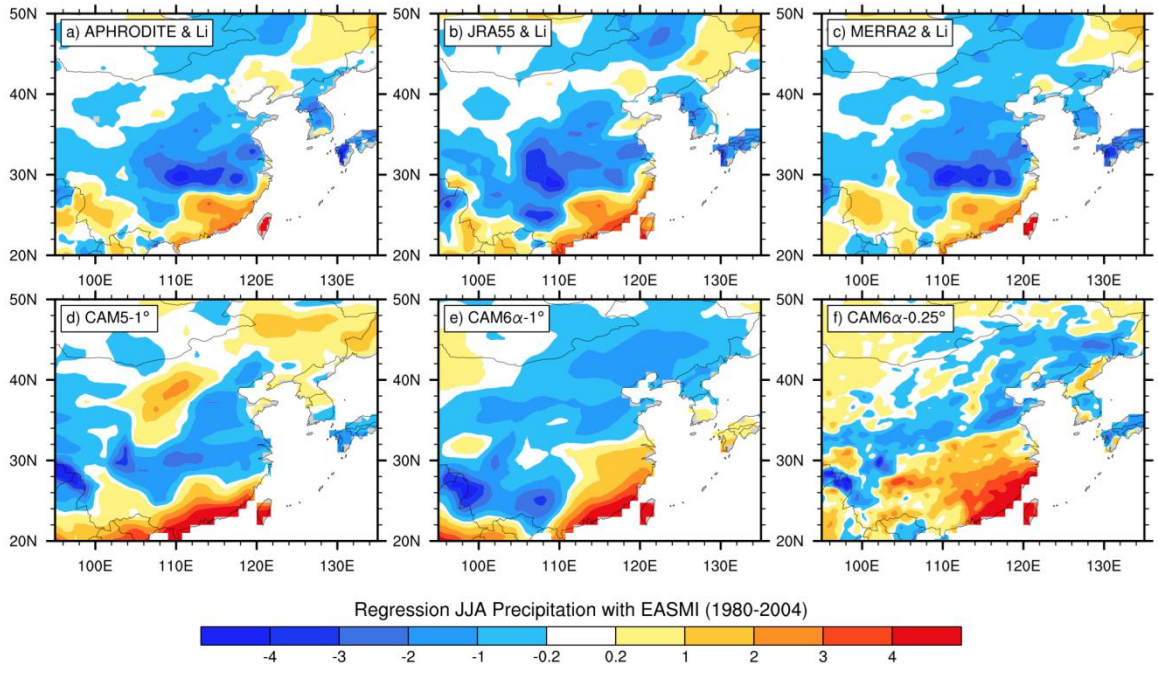

Figure 8. Summer (JJA) precipitation regressed onto EASMI (mm/day) for 1980-2004.

Geosci. Model Dev. Discuss., https://doi.org/10.5194/gmd-2019-1
Manuscript under review for journal Geosci. Model Dev.
Discussion started: 28 January 2019

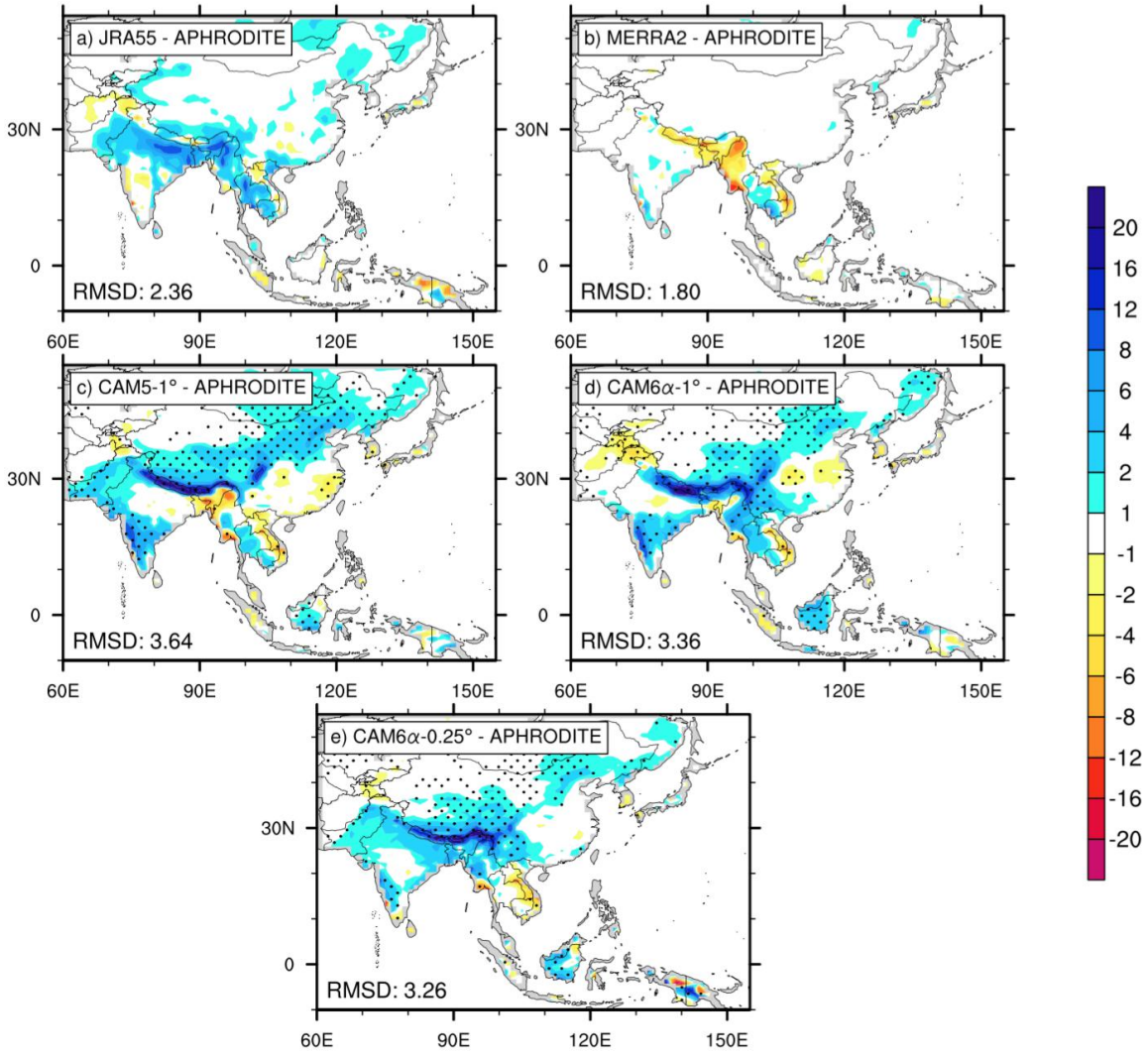

Figure 9. The difference of summer minus winter (JJA - DJF) precipitation (mm/day) between APHRODITE and a) JRA55, b) MERRA2, c) CAM5-1˚, d) CAM6α-1˚ and e) CAM6α-0.25˚, respectively. The values at the lower left of every panel indicate the root mean squared difference (RMSD) relative to APHRODITE.

Geosci. Model Dev. Discuss., https://doi.org/10.5194/gmd-2019-1
Manuscript under review for journal Geosci. Model Dev.
Discussion started: 28 January 2019

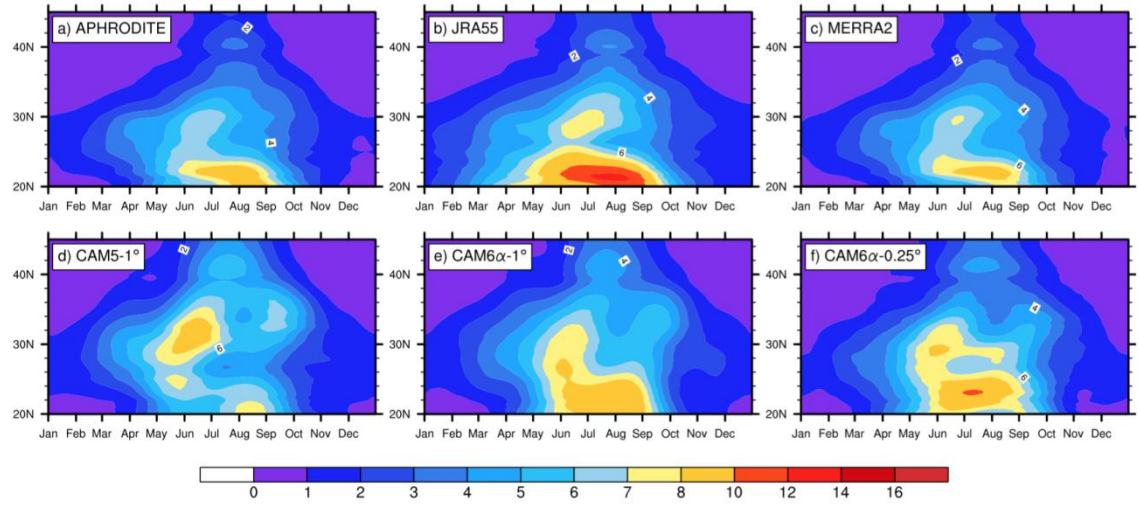

Figure 10. Annual cycle of regional mean precipitation rate (mm/day) for 1980-2004 within Southern China (between 100˚E and 125˚E): a) APHRODITE, b) JRA55, c) MERRA2, d) CAM5-1˚, e) CAM6α-1˚ and f) CAM6α-0.25˚.

Geosci. Model Dev. Discuss., https://doi.org/10.5194/gmd-2019-1
Manuscript under review for journal Geosci. Model Dev.
Discussion started: 28 January 2019

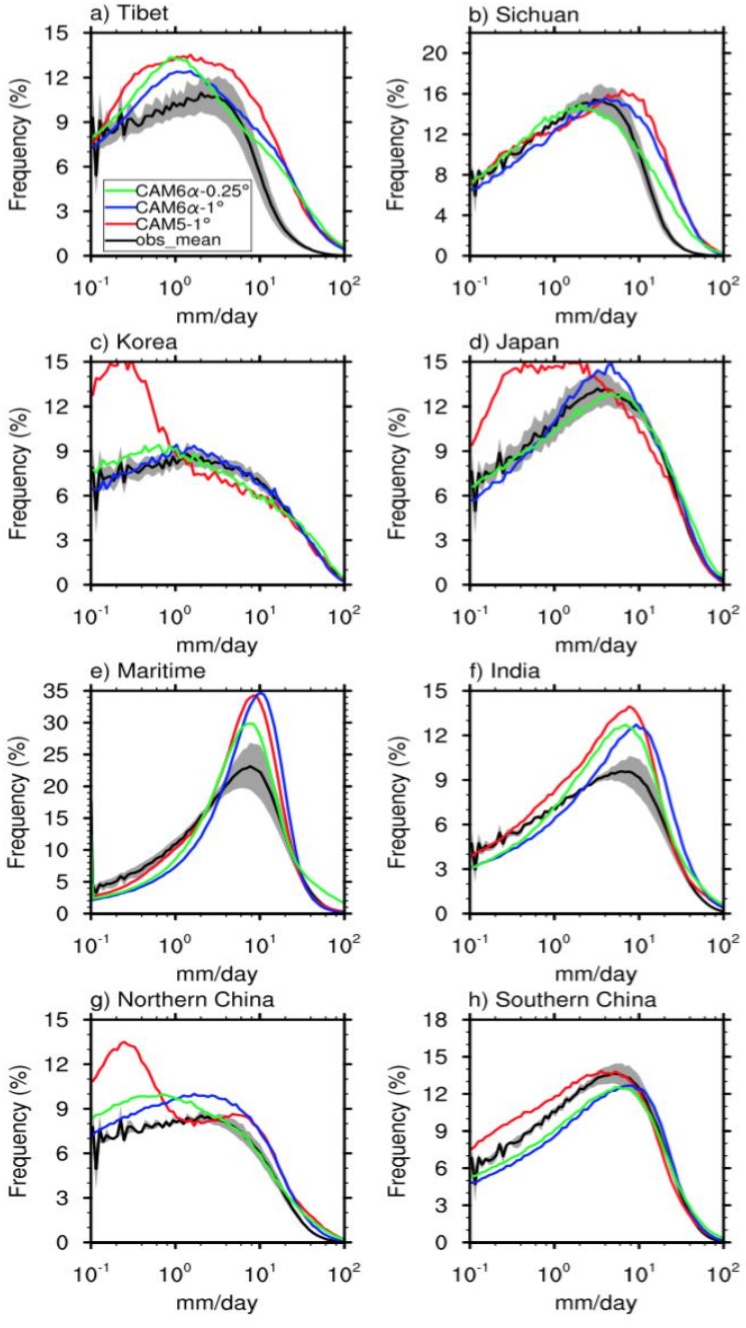

Figure 11. Frequency distribution of daily precipitation (mm/day) over a) Tibet, b) Sichuan, c) Korea, d) Japan, e) maritime continent (see boxes in Figure 2.c), f) India, g) Northern China and h) Southern China for 1980-2004. Black lines (shading) for the mean (one standard deviation) of APHRODITE, JRA55 and MERRA2. Red solid lines for CAM5-1°; blue solid lines for CAM6α-1°; green solid lines for CAM6α-0.25°.

Geosci. Model Dev. Discuss., https://doi.org/10.5194/gmd-2019-1
Manuscript under review for journal Geosci. Model Dev.
Discussion started: 28 January 2019

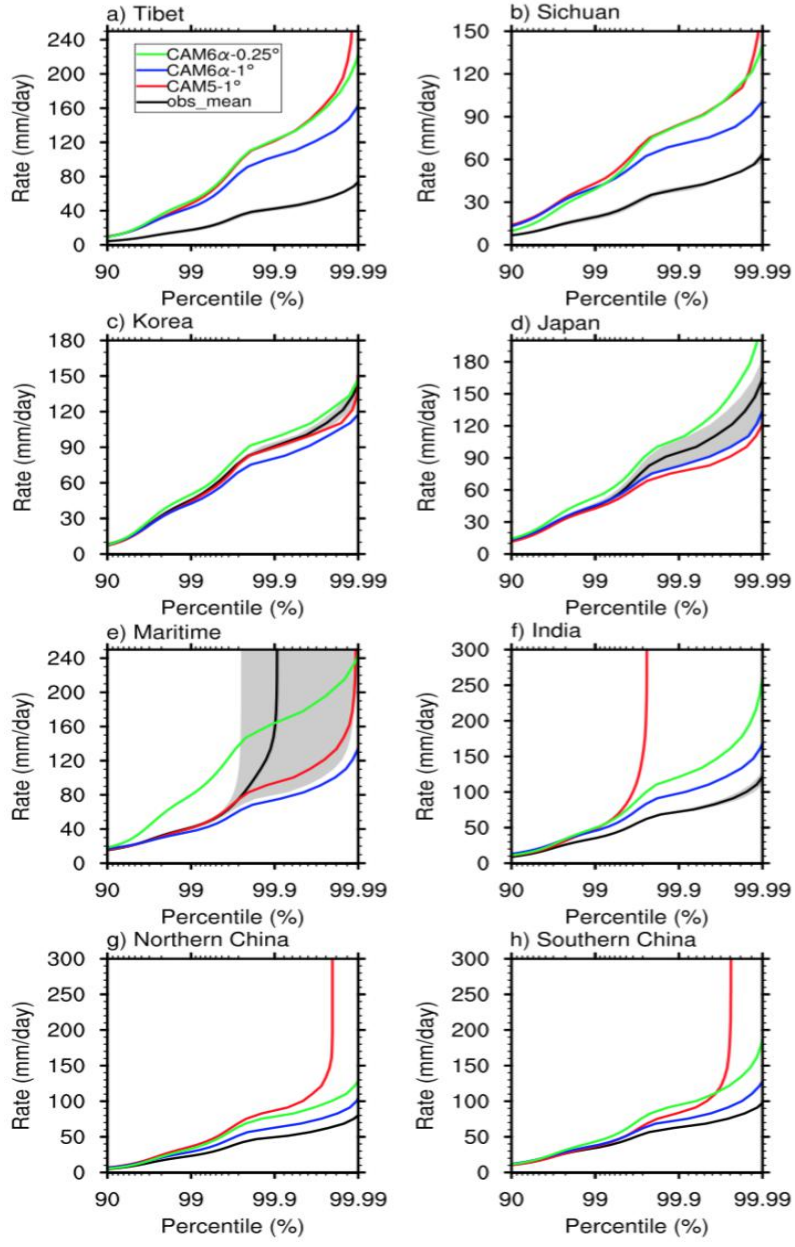

Figure 12. Similar to Figure 11, but for daily precipitation rates (mm/day) as a function of percentile.

Geosci. Model Dev. Discuss., https://doi.org/10.5194/gmd-2019-1
Manuscript under review for journal Geosci. Model Dev.
Discussion started: 28 January 2019

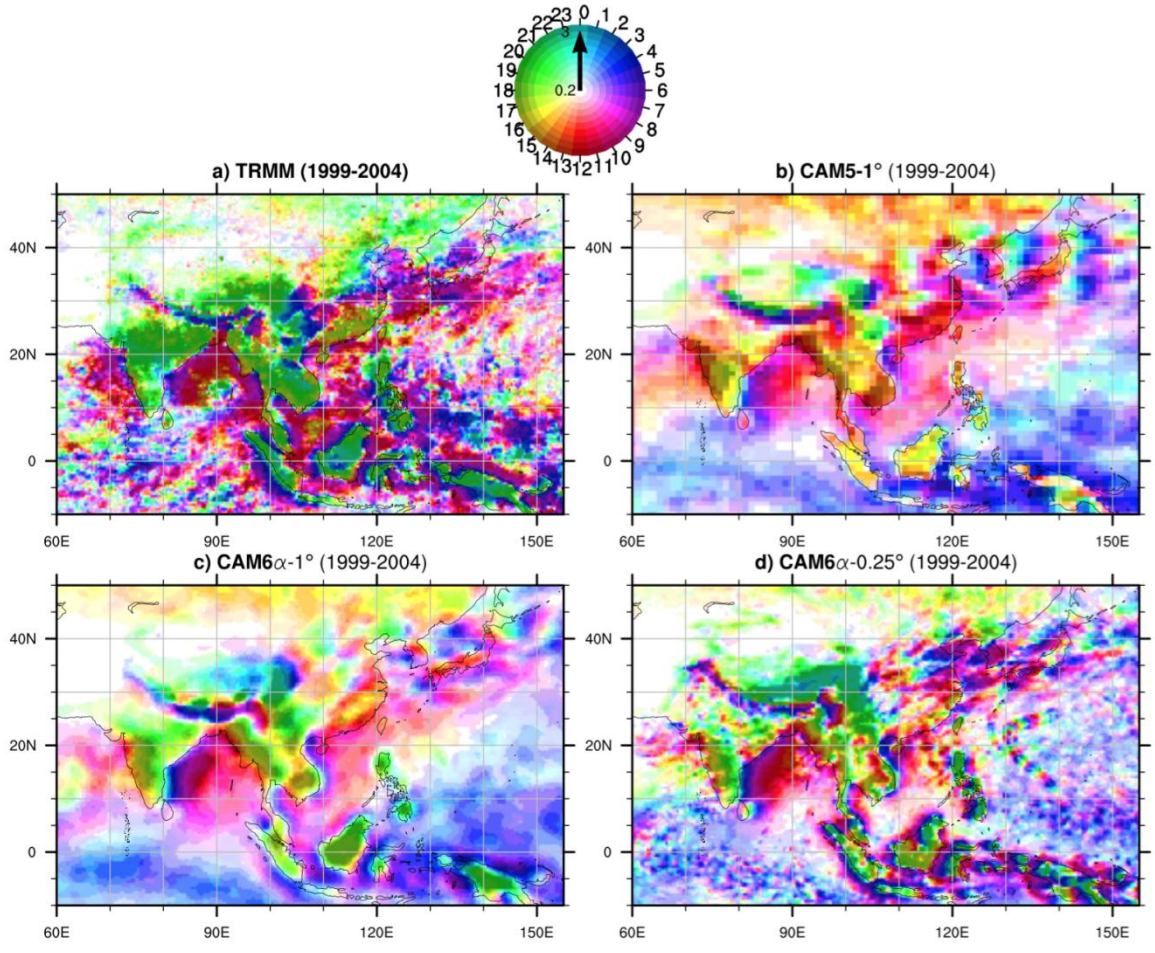

Figure 13. Diurnal cycle of precipitation in June (6-year average from 1999-2004) of (a) TRMM, (b) CAM5-1º, (c) CAM6α-1º and (d) CAM6α-0.25º. The local time peak of the diurnal cycle is shown in color on the color wheel. The intensity of the color is the amplitude of precipitation.

Geosci. Model Dev. Discuss., https://doi.org/10.5194/gmd-2019-1
Manuscript under review for journal Geosci. Model Dev.
Discussion started: 28 January 2019

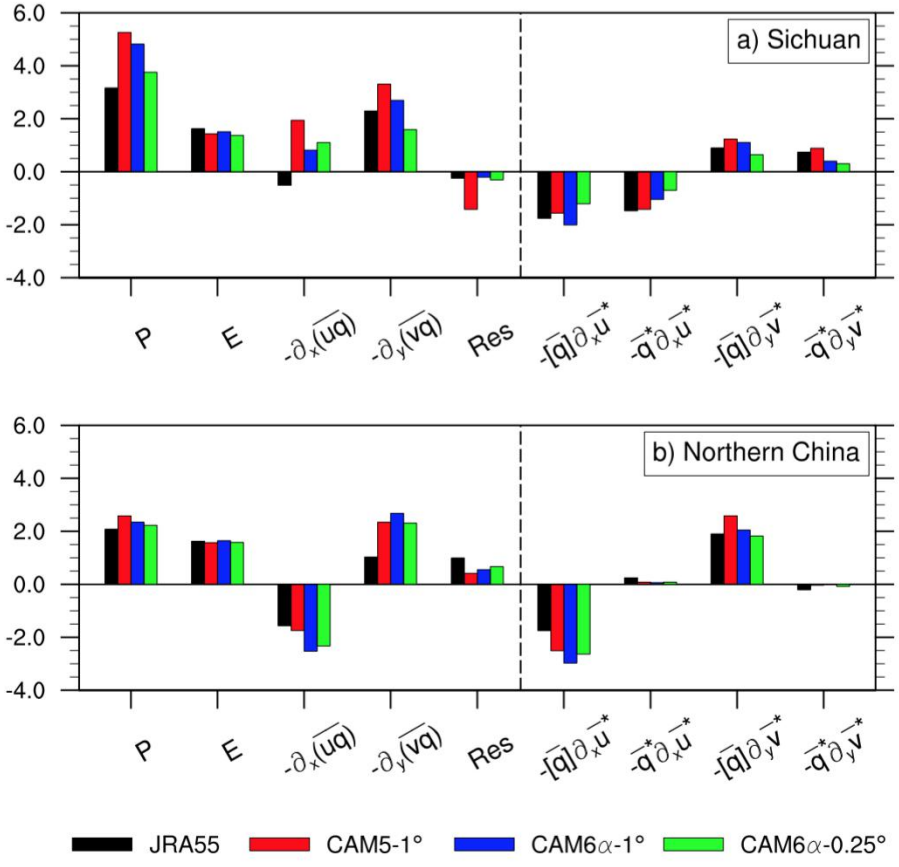

Figure 14. Moisture budget over a) Sichuan and b) Northern China (see the boxes of Figure 2c) for 1980-2004, including precipitation, evaporation, zonal and meridional moisture flux convergence, residual and (right to dashed line) major processes contributing to moisture flux convergence.